Theory and modeling of light interactions with metallic nanostructures

2008 J. Phys.: Condens. Matter 20 323201

(http://iopscience.iop.org/0953-8984/20/32/323201)

IOP PUBLISHING JOURNAL OF PHYSICS: CONDENSED MATTER

J. Phys.: Condens. Matter **20** (2008) 323201 (11pp) doi:10.1088/0953-8984/20/32/323201

TOPICAL REVIEW

Theory and modeling of light interactions with metallic nanostructures

Jason M Montgomery[1], **Tae-Woo Lee**[2] **and Stephen K Gray**[1]

[1] Chemical Sciences and Engineering Division, Argonne National Laboratory, Argonne, IL 60439, USA

[2] Center for Computation and Technology, Louisiana State University, Baton Rouge, LA 70803, USA

Received 31 January 2008, in final form 4 June 2008
Published 18 July 2008
Online at stacks.iop.org/JPhysCM/20/323201

Abstract

Metallic nanostructures such as systems containing metal nanoparticles or nanostructured metal films are intriguing systems of much current interest. Surface plasmons, i.e., special electronic excitations near the metallic surfaces, can then be excited in these systems. Surface plasmons can be intense and localized, and correctly describing their behavior in complex systems can require numerically rigorous modeling techniques. The finite-difference time-domain (FDTD) method is one such technique. This review discusses results obtained mostly with the FDTD method concerning (i) local surface plasmon excitations of metal nanoparticles, (ii) surface plasmon polariton propagation on layered structures, (ii) and periodic hole arrays in metal films.

(Some figures in this article are in colour only in the electronic version)

Contents

1. Introduction

Metallic nanostructures, including metal nanoparticles, nanostructured metal films, and more complex structures containing additional materials have been the focus of much recent attention [1–4]. Surface plasmons (SPs) can be optically excited in such systems. SPs [5, 6], collective excitations of electrons near the metal surfaces, can be localized and very intense near the surface (see figure 1). The properties of SPs make metallic nanostructures interesting for a variety of applications in optics, chemical and biological sensing and optoelectronics. A variety of acronyms are used in this review and table 1 collects them all for easy reference.

Insight into the nature of SPs can be garnered from inspection of the exact analytical solutions of Maxwell's equations available for certain problems such as Mie's solution for light scattering by a sphere of arbitrary complex-valued dielectric constant [6, 7]. Approximate analytical solutions valid in certain limits, such as the quasistatic limit of wavelength, λ, much smaller than particle dimensions, are also instructive. The quasistatic limit result for the polarizability, α, of a small spherical particle of radius a [6, 8] exposed to an electric field with angular frequency ω is

$$\alpha = 4\pi a^3 \frac{\varepsilon_m(\omega) - \varepsilon_{med}}{\varepsilon_m(\omega) + 2\varepsilon_{med}}, \quad (1)$$

where the dielectric constant within the sphere is $\varepsilon_m(\omega)$ and the relative dielectric constant of the medium outside the sphere

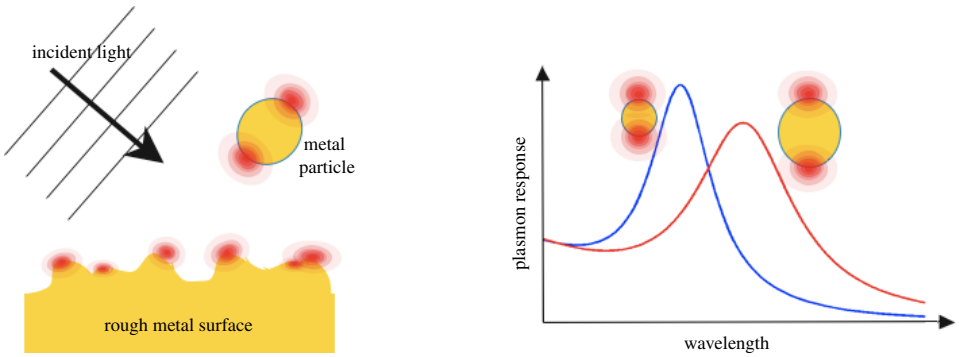

Figure 1. Schematic illustration of local surface plasmon excitations on metal nanoparticles and rough metal surfaces. The electromagnetic field intensity (red online, gray in print) can be high and localized near the metal surfaces. The plasmon response, e.g. an optical cross section in the case of nanoparticles, is size dependent.

Table 1. Acronyms used throughout the text and their corresponding meanings.

SP	Surface plasmon
SPP	Surface plasmon polariton
LSP	Localized surface plasmon
LR-SPP	Long range surface plasmon polariton
FDTD	Finite difference time domain
DDA	Discrete dipole approximation
PML	Perfectly matched layer
UPML	Uniaxial perfectly matched layer
ADE	Auxiliary differential equation
TF	Total field
SF	Scattered field
TFSF	Total field/scattered field
MNP	Metal nanoparticle
SERS	Surface enhanced Raman spectroscopy
TM	Transverse magnetic
ATR	Attenuated total reflection
EOT	Extraordinary optical transmission
TEM	Tunneling electron microscopy
RI	Refractive index

is ε_{med}. The absorption cross section is proportionate to $\text{Im}(\alpha)$, and the magnitude of the scattered electric field outside the particle is dominated by $|\alpha|/a^3$. The localized surface plasmon (LSP) resonance for the particle is associated with maxima in the optical cross sections or when $\text{Re}[\varepsilon_{\text{m}}(\omega)] = -2\varepsilon_{\text{med}}$. Since ε_{med} is generally positive, the LSP is associated with a negative real part of the dielectric constant. Silver and gold are popular materials to use in metallic nanostructures owing to the fact that they have negative real parts to their dielectric constants in the visible spectral region. LSPs may be thought of as the electromagnetic analog of quantum mechanical bound states.

Also of relevance are also traveling surface plasmons that can be excited on metal films, which are called surface plasmon polaritons (SPPs) [5]. If one considers a thin metal film sitting on top of a substrate of relative dielectric constant ε_{s} with a less optically dense medium above ($\varepsilon_{\text{med}} < \varepsilon_{\text{s}}$), then the SPP wavevector for propagation along the surface is given by [5]

$$k_{\text{SPP}}(\omega) = \frac{\omega}{c}\left(\frac{\varepsilon_{\text{med}}\varepsilon_{\text{m}}(\omega)}{\varepsilon_{\text{med}} + \varepsilon_{\text{m}}(\omega)}\right)^{1/2}, \tag{2}$$

and it is possible to couple into such SPPs by passing light at an appropriate angle up through the substrate to achieve wavevector matching. In order to be an evanescent surface wave that decays in the medium away from the metal surface, the SPP must have $\text{Re}[k_{\text{SPP}}] = \omega/c$, which for ordinary media with positive dielectric constants requires $\text{Re}[\varepsilon_{\text{m}}] < 0$.

The analysis above and its various extensions are very useful for understanding the basic properties of SPs [1, 2, 5, 6, 8], as well as developing ideas for exploiting SPs in more complex nanostructures. However, in order to validate such ideas, to predict optimal nanostructures for specific uses, and to explore emergent phenomena not evident from simpler considerations, more rigorous electrodynamics calculations are required. The purpose of this topical review is to discuss, with some emphasis on the finite-difference time-domain method [9, 10], a variety of studies of light interacting with metallic nanostructures.

2. Finite-difference time-domain method

The primary computational tool used in much of the work discussed here is the finite-difference time-domain (FDTD) method [9, 10]. This method has the advantages that it can be applied to a variety of complex problems and one time propagation can provide information about a wide range of frequencies. It is also the case that, while it can be computationally demanding, the core algorithm is sufficiently simple and can be efficiently implemented on parallel computers. Three-dimensional, full vector simulations with the FDTD method are becoming more and more routine. Nonetheless it is important to note that there are also a variety of frequency-domain methods that can provide numerically accurate results. The discrete dipole approximation (DDA) [11], for example, has proved to be very efficient and reliable for obtaining the optical properties of metal nanoparticles [8, 12]. Other frequency-domain approaches that have seen use in problems involving surface plasmons include the multiple multipole method [13], integral equation approaches [14, 15], and the vector finite element method [16].

The FDTD method is a numerical method for solving the time-domain Maxwell's equations for spatiotemporal evolution of the electric and magnetic fields. It involves representing the fields on (staggered) grids and a leap-frog scheme for

taking discrete time steps. These relatively simple, basic ideas were given by Yee in his seminal 1966 paper [9]. Efficient and accurate simulations of metallic nanostructures, however, require some sophisticated embellishments to the basic approach. The book by Taflove and Hagness details these more modern developments [10].

2.1. Maxwell's time-domain equations and dielectric dispersion

A convenient form of Maxwell's time-domain equations for modern implementations of the FDTD method, with metallic nanostructures in mind, is the general form,

$$\frac{\partial \mathbf{D}(t)}{\partial t} = \nabla \times \mathbf{H}(t), \tag{3}$$

$$\frac{\partial \mathbf{B}(t)}{\partial t} = -\nabla \times \mathbf{E}(t), \tag{4}$$

which involves four three-component vectors, $\mathbf{D}(t)$, $\mathbf{E}(t)$, $\mathbf{B}(t)$, and $\mathbf{H}(t)$, each of which depends on the three spatial Cartesian coordinates x, y and z. The optical and magnetic response of a material occupying a given spatial region allows one to relate $\mathbf{D}$ to $\mathbf{E}$ and $\mathbf{B}$ to $\mathbf{H}$, thus completing the system of equations to be solved. These relations are called constitutive relations. The noble metal nanostructures frequently of interest in plasmonics can be considered non-magnetic so that $\mathbf{B}(t) = \mu_0 \mathbf{H}(t)$, and one can eliminate $\mathbf{B}(t)$ from the equations. (However, a useful embellishment of the FDTD method for absorbing outgoing waves at the grid edges does involve an artificial magnetic aspect. See section 2.3.)

For ordinary, non-dispersive dielectric materials, $\mathbf{D}(t) = \varepsilon_r \varepsilon_0 \mathbf{E}(t)$, with ε_r being the relative dielectric constant such that the material's refractive index is $[\varepsilon_r]^{1/2}$. However, for the metals of interest, ε_r is complex-valued and dispersive, i.e., depends on frequency in the frequency-domain version of Maxwell's equations. In order to account for these features in the time domain, it is convenient to first define the constitutive relation for $\mathbf{D}$ in the frequency domain as

$$\mathcal{D}(\omega) = \varepsilon_0 \varepsilon_r(\omega) \mathcal{E}(\omega) = \varepsilon_0 \left(\varepsilon_\infty + \sum_j \frac{A_j}{\omega_j^2 - \omega^2 - i\gamma_j \omega} \right) \mathcal{E}(\omega), \tag{5}$$

where $\varepsilon_r(\omega)$ is expressed as a general n-pole Lorentzian model [6], which treats electrons as a collection of n different types of coupled harmonic oscillators and calculates their response to a time-harmonic field with angular frequency ω. Here ε_∞ represents the high-frequency limit, and for the jth type of oscillator, ω_j is the resonant frequency and γ_j is a damping constant giving rise to absorption. Lorentzian terms can be thought of as describing the extent to which electrons are bound. In order to describe the motion of free electrons within a metal, a Drude model is obtained by setting $\omega_j = 0$. In practice, the parameters ε_∞, A_j, ω_j, and γ_j ($j = 1, 2, \ldots, n$) are optimized to fit $\varepsilon_r(\omega)$ to the empirical dielectric constant data inferred from, e.g., thin film transmission measurements [17, 18]. The number of Drude and Lorentzian terms necessary to obtain an accurate fit over a range of frequencies may vary. For silver at optical wavelengths, for example, one Drude and two Lorentzian terms are usually sufficient, as illustrated in figure 2.

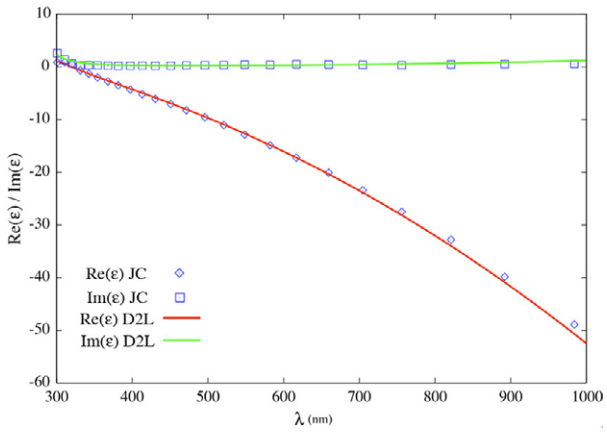

Figure 2. Comparison of the empirical dielectric constant data (symbols) for silver of Johnson and Christy (JC) [17] with an analytical Drude + 2 Lorentzian (D2L) model fit (curves) over the 300–1000 nm wavelength range.

Equation (5) can be re-written in terms of polarization terms, $\mathcal{P}_j(\omega)$, such that

$$\varepsilon_0 \left(\sum_j \frac{A_j}{\omega_j^2 - \omega^2 - \mathrm{i}\gamma\omega} \right) \mathcal{E}(\omega) = \sum_j \mathcal{P}_j(\omega). \tag{6}$$

Fourier transformation of equation (6) then leads to the time-dependent constitutive relation for obtaining $\mathbf{E}$ from $\mathbf{D}$:

$$\mathbf{E}(t) = \frac{1}{\varepsilon_0 \varepsilon_\infty} \left(\mathbf{D}(t) - \sum_j \mathbf{P}_j(t) \right). \tag{7}$$

An auxiliary differential equation, or ADE [10, 19], is obtained for the jth term $\mathbf{P}_j(t)$ in equation (7) by Fourier transforming equation (6):

$$\frac{\partial^2 \mathbf{P}_j(t)}{\partial t^2} + \gamma_j \frac{\partial \mathbf{P}_j(t)}{\partial t} + \omega_j^2 \mathbf{P}_j(t) = \varepsilon_0 A_j \mathbf{E}_j(t), \tag{8}$$

where the relation $(-\mathrm{i}\omega)^n \rightarrow \partial^n / \partial t^n$ was used, given a time-dependent factor $\exp(-\mathrm{i}\omega t)$. The FDTD method then corresponds to a numerical method for solving equations (3), (4) and (8), given equation (7). Of course one could, with equation (5), eliminate $\mathbf{D}$ from consideration as in [19]. However, given the absorption procedure frequently used, section 2.3, it is sometimes convenient to keep it. In the case of just a Drude metal being present, the procedure is simpler [20].

2.2. The Yee algorithm core

The core discretization and propagation scheme behind the FDTD method was first presented in Yee's seminal paper [9]. It consists of a leap-frog time propagation which is second order accurate in time. It achieves second order accuracy in spatial derivatives in an efficient manner with staggered grids

and is such that, in free space, Gauss's and Ampere's laws are satisfied [10]. For simplicity of presentation, however, we forgo a detailed presentation of the spatial derivative expressions and focus on the time stepping component of the FDTD method.

For a constant time spacing Δt, the nth time step begins with updating $\mathbf{D}(t)$ in equation (3):

$$\begin{aligned} D_x\big|^{n+1/2} &= D_x\big|^{n-1/2} + \Delta t\left(\frac{\partial H_z}{\partial y}\bigg|^{n} - \frac{\partial H_y}{\partial z}\bigg|^{n}\right), \\ D_y\big|^{n+1/2} &= D_y\big|^{n-1/2} + \Delta t\left(\frac{\partial H_x}{\partial z}\bigg|^{n} - \frac{\partial H_z}{\partial x}\bigg|^{n}\right), \\ D_z\big|^{n+1/2} &= D_z\big|^{n-1/2} + \Delta t\left(\frac{\partial H_y}{\partial x}\bigg|^{n} - \frac{\partial H_x}{\partial y}\bigg|^{n}\right), \end{aligned} \tag{9}$$

where $D_x|^{n+1/2} = \mathbf{D}(x, y, z, (n+1/2)\Delta t)$, etc.

Next, each relevant polarization vector $\mathbf{P}_j|^{n+1/2}$ is updated using $\mathbf{P}_j|^{n-1/2}$, $\mathbf{P}_j|^{n-3/2}$, and $\mathbf{E}|^{n-1/2}$, with

$$\begin{aligned} \mathbf{P}_j\big|^{n+1/2} = &\left(\frac{2-(\omega_j\Delta t)^2}{1+\gamma_j\Delta t/2}\right)\mathbf{P}_j\big|^{n-1/2} \\ &- \left(\frac{1-\gamma_j\Delta t/2}{1+\gamma_j\Delta t/2}\right)\mathbf{P}_j\big|^{n-3/2} + \left(\frac{\varepsilon_0 A_j\Delta t^2}{1+\gamma_j\Delta t/2}\right)\mathbf{E}|^{n-1/2}, \end{aligned} \tag{10}$$

which is a re-arranged form of the finite-difference analog of equation (8). Now $\mathbf{E}|^{n+1/2}$ can be obtained easily via

$$\mathbf{E}|^{n+1/2} = \frac{1}{\varepsilon_0\varepsilon_\infty}\left(\mathbf{D}|^{n+1/2} - \mathbf{P}|^{n+1/2}\right), \tag{11}$$

where $\mathbf{P}|^{n+1/2}$ is the total polarization vector.

Updates for the components of $\mathbf{B}$ are given by

$$\begin{aligned} B_x\big|^{n+1} &= B_x\big|^{n} + \Delta t\left(\frac{\partial E_y}{\partial z}\bigg|^{n+1/2} - \frac{\partial E_z}{\partial y}\bigg|^{n+1/2}\right), \\ B_y\big|^{n+1} &= B_y\big|^{n} + \Delta t\left(\frac{\partial E_z}{\partial x}\bigg|^{n+1/2} - \frac{\partial E_x}{\partial z}\bigg|^{n+1/2}\right), \\ B_z\big|^{n+1} &= B_z\big|^{n} + \Delta t\left(\frac{\partial E_x}{\partial y}\bigg|^{n+1/2} - \frac{\partial E_y}{\partial x}\bigg|^{n+1/2}\right). \end{aligned} \tag{12}$$

If the material is non-magnetic, then $\mathbf{H}$ (for use at the start of the next time step) is simply

$$\mathbf{H}\big|^{n+1} = \frac{1}{\mu_0}\mathbf{B}\big|^{n+1}, \tag{13}$$

and the process is repeated. It is useful to note that using a total of n Drude and/or Lorentzian terms results in n ADEs to propagate and $2n$ additional $\mathbf{P}_j$ arrays to store. To alleviate computational effort, solution of these n additional equations may be restricted to metallic regions of space.

2.3. Absorbing boundary conditions and source injection

The implementation of absorbing boundary conditions at the edges of the FDTD grid is very important since otherwise outgoing waves will be artificially reflected back into the physical region. The most straightforward approach is to define an absorbing layer around the grid and to damp the fields in this layer after each time step [20]. Unfortunately, this requires the use of a relatively large absorbing layer in order to avoid artificial reflections and so is not practical for three-dimensional simulations. Other approaches with varying degrees of complexity are reviewed in [10]. Two excellent approaches are Berenger's perfectly matched layer (PML) [10, 21] and Gedney's uniaxial anisotropic perfectly matched layer (UPML) [19, 22]. Both are consistent with the introduction of an artificial absorbing medium and involve impedance matching ideas to minimize reflection errors. For the PML, the electric and magnetic field components are split into subcomponents within the absorbing region and additional electric/magnetic conductivities are introduced. The UPML, on the other hand, does not split the $\mathbf{E}$ fields but introduces certain constitutive relations relating $\mathbf{D}$ to $\mathbf{E}$ and $\mathbf{B}$ and $\mathbf{H}$ in the absorbing region consistent with a dispersive, complex, absorbing medium in the frequency domain. An ADE approach similar in spirit to that of section 2.2 is used to implement the UPML. Much of our own work has involved use of UPMLs, which we have also found can be applied across metallic regions in order to simulate infinitely extended metal regions.

The total-field/scattered-field (TFSF) approach [10, 23] is a useful method for injecting arbitrary source fields into the FDTD grid. A TFSF boundary is specified within the computational grid, separating an inner total-field (TF) region from an outer scattered-field (SF) region. Special attention is paid to those grid points directly located on either side of a TFSF boundary. For example, the FDTD update equations for a grid point in the TF region located adjacent to a TFSF boundary involve field components on a neighboring SF grid point. Values of the incident field must then be added to the SF point during the FDTD update. A similar treatment is performed for the FDTD updates on SF grid points adjacent to the TFSF boundary, in which the incident field on the neighboring TF grid point must be subtracted during the FDTD update. In such a manner, an incident wave of arbitrary length, direction and shape can easily be introduced into an FDTD calculation without the use of large grids.

3. Illustrative studies

3.1. Local surface plasmon excitations in metal nanoparticles

The nature of the interaction of light with metallic nanoparticles (MNPs), the role of SPs, and their characteristic optical properties have been the focus of much experimental and theoretical research. One can attempt to tailor the scattering and absorbing cross sections, as well as near-field enhancements, by varying the size, shape, composition, and dielectric environment of MNP structures, making them viable candidates for nanoscale optics, optoelectronics, and chemical and biological sensing devices. Accordingly, one needs accurate theoretical methods for characterizing and even designing such devices. Analytical treatments based on Mie's

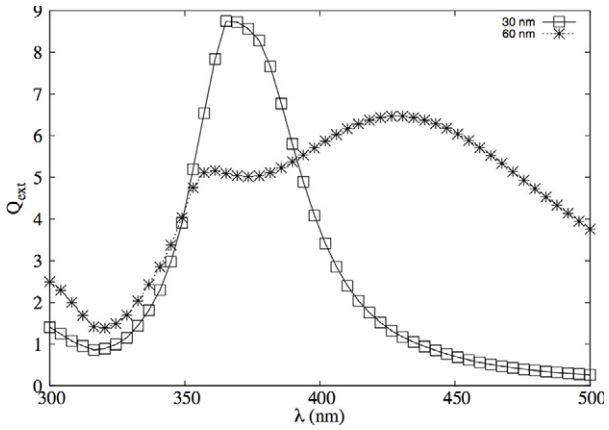

Figure 3. Extinction efficiencies for 30 and 60 nm Ag spheres using Mie's analytical solution to Maxwell's equations. The dielectric constant for Ag is based on the Lynch and Hunter [18] empirical data. For the 30 nm particle, a sharp dipole resonance peak is seen at ∼365 nm. For the 60 nm particle, the dipole resonance peak is red shifted to ∼427 nm, while a quadrupole peak is seen at ∼361 nm.

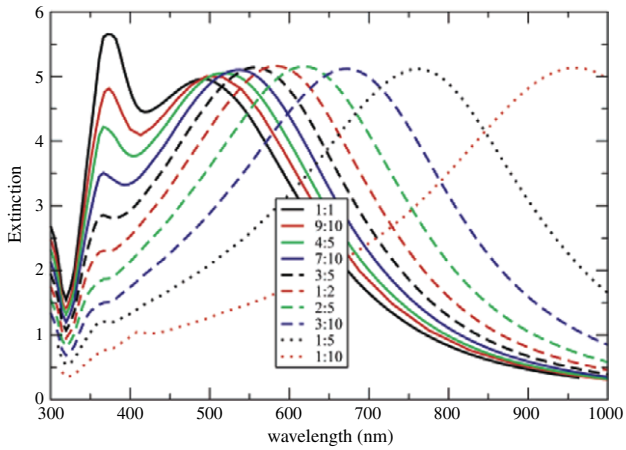

Figure 4. Results of exact numerical calculations of the extinction spectra of oblate spheroids, all with volume corresponding to an 80 nm sphere, with incident light polarized along the major axis. The major to minor axis aspect ratio, a/b, is varied from 1 to 10. The main dipole resonance red shifts with increasing aspect ratio and the quadrupole peak is quenched. Reprinted figure with permission from [8]. Copyright 2003 by The American Chemical Society.

solutions have remained quite useful due to the fact that many colloid prepped nanoparticles are roughly spherical. The advent of new chemical and physical techniques, such as e-beam lithography, capable of making very precise shapes (spheres, prisms, shells, cubes, bipyramids, rods, triangles, tetrahedrons, hybrid core–shell structures, etc) as well as advancements in scientific computing have helped spur more recent theoretical work. Another complicating factor that Mie theory is not able to address but which is of utmost importance for the realization of nanophotonic devices is the interaction between particles and other particles or substrates. For this reason, the use of more accurate numerical techniques, such as the FDTD method described in section 2, and other accurate methods such as the DDA method [8, 11, 12], have been paramount. In this section, we present a brief account of several studies involving the use of these analytical and numerical methods to calculate the optical properties (namely extinction and scattering efficiencies and field enhancements) for various MNP structures.

Spheres and spheroids. We begin with a look at silver nanospheres with radius r. Although simple in structure, the nature of SPs for spheres and their dependence on size provide useful insights into the more complicated MNP structures. In [8], Kelly *et al* give a helpful review of the analytical treatment of light scattering by spherical MNPs. Specifically, they present expressions for extinction (Q_{ext}) and scattering (Q_{sca}) efficiencies, which include both dipole and quadrupole type plasmon resonances. Using empirical values for the dielectric constant of silver, $\varepsilon_{\text{Ag}}(\lambda)$ [18], over a wavelength range of $\lambda = 300$–500 nm, they calculate and plot $Q_{\text{ext}}(\lambda)$ for $r = 30$ and 60 nm silver spheres (see figure 3). For the $r = 30$ nm sphere, a single, sharp peak is seen at $\lambda = 365$ nm, corresponding to a dipole plasmon resonance. For the $r = 60$ nm sphere, the dipole resonance is broadened and red shifted approximately 62 nm. Furthermore, a noticeable quadrupole resonance is now present at $\lambda = 357$ nm. A look at electric intensity enhancements, $|E|^2/|E_0|^2$, verifies assignments of dipole and quadrupole resonance peaks and shows a maximum intensity enhancement of nearly 100 for the $r = 30$ nm sphere and 35 for the $r = 60$ nm sphere.

In addition, Kelly *et al* present a similar analytical treatment for spheroids but invoke the quasistatic approximation ($\lambda \gg r$) with a modified long wavelength approximation correction, as well as numerical results based on the more complex, exact analytical solutions for spheroids [8]. Due to the loss of spherical symmetry in a spheroid, polarization of incident light becomes an important factor. For both oblate and prolate spheroids associated with a given aspect ratio a/b of major to minor axes, two resonances are seen each associated with the orientation of light being polarized along either a major axis (resonance is red shifted as a/b is increased) or a minor axis (resonance is blue shifted as a/b is increased). These analytical treatments then are ideal to show the sensitivity that optical properties of SPs exhibit with both size and shape. Figure 4, for example, shows the shape-dependent red-shifting of the dipolar resonance as the aspect ratio is increased. The quadrupole resonance, which exists to the red of the dipole resonance for the spherical limit ($a/b = 1$) is quenched with increasing aspect ratio.

Rods, bipyramids, and triangular prisms. As noted above, recent advances in fabrication of MNPs allow for size tunability of some very specific, non-spherical shapes. As a non-trivial example of how size and shape can affect the nature of SPs in MNPs, we look to a study of rod-like and bipyramidal gold nanoparticles by Liu *et al* [24]. With such structures, the aspect ratio, a/b, is an adjustable parameter that can strongly affect the nature of plasmon resonances. Liu *et al* focus on variations in the optical spectra and field enhancements of rod-like structures (cylinders capped with hemispheres) for three increasing aspect ratios, $a/b = 3.4$, 4.1, and 4.8, for

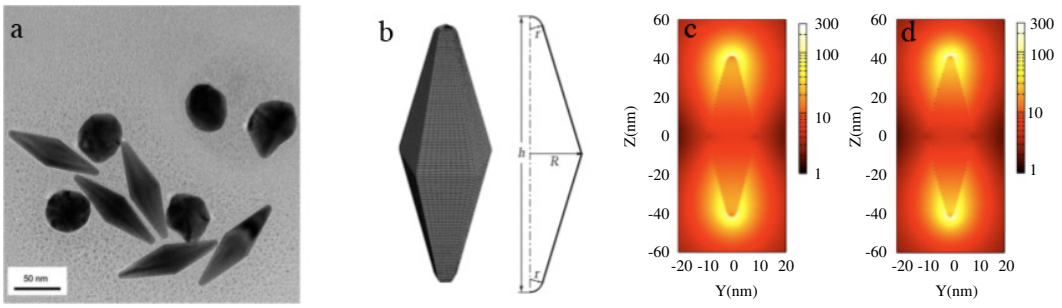

Figure 5. (a) TEM image of gold pentagonal bipyramids (with some spherical particles also present). (b) 3D pictorial representation of the structure considered in the FDTD calculations. (c) FDTD-calculated field enhancement, $|E|/|E_0|$, for a bipyramid with $R = 15$ nm, $h = 83.4$ nm, and tip radius of curvature $r = 3$ nm. Field propagation is in the x direction with incident light at the plasmon resonance polarized in the z direction. (d) Similar to (c) but with $r = 2$ nm (more pointed tips). Reprinted figure with permission from [24]. Copyright 2007 by The American Physical Society.

a fixed 14 nm diameter. Experimental and FDTD absorption efficiencies are in good agreement and show a red shift and spectral broadening in the longitudinal plasmon resonance for increasing a/b (see figure 5 in [24]). Field enhancements, $|E|/|E_0|$, for $a/b = 4.1$ were calculated to be approximately 35 at the extremities, giving rise to intensity enhancements, $|E|^2/|E_0|^2$, of nearly 1225.

In [24], a similar study was performed for pentagonal bipyramids. Figure 5(a) contains a TEM image of gold bipyramids fabricated in aqueous solution (with spherical gold particles also present), and (b) contains the 3D FDTD structure modeled, with a base radius $R = 15$ nm, height $h = 83.4$ nm, and a variable tip radius of curvature $r = 4.4$ nm, 3.0, or 2.0 nm. For light polarized in the longitudinal (along h) direction, FDTD calculations show that a red shift and broadening is seen in the plasmon resonance wavelength for increasing sharpness (i.e. as r decreases). Figures 5(c) and (d) contain FDTD results of the strong field enhancement for $r = 3$ nm and $r = 2$ nm, respectively. Although not evident from the figure, it can be shown that maximum field enhancement increases with increasing sharpness, with $|E/|E_0| \approx 140$ for $r = 3$ nm and $|E|/|E_0| \approx 200$ for $r = 2$ nm. Such strong near-field enhancements make the gold bipyramidal MNPs very good candidates for use in surface enhanced Raman scattering (SERS) type applications [8, 12], where the SERS enhancement would be on the order of $(|E|/|E_0|)^4 = 200^4$. It is also useful to note that the *inner* field enhancements for the bipyramidal structures considered are nearly 30 near the surface (as opposed to 10 within similar sized spheres and 6 within the rod-like structures). These results also suggest that gold bipyramidal MNPs would be useful candidates for obtaining and studying optical nonlinearity effects.

In [8, 25], the frequency-domain DDA method is used to calculate $Q_{\text{ext}}(\lambda)$ and $|E|/|E_0|$ for silver triangular prisms exhibiting varying degrees of tip truncations: $s = 0$, 5, and 10 nm, where s measures the distance at which the tip is clipped (see figure 6). The perfect triangle ($s = 0$) consisted of 100 nm edges and a 16 nm thickness, and an analysis of three distinct peaks seen in Q_{ext} (λ) reveal a strong dipole resonance, which for increasing values of s is blue shifted, and two small but significant quadrupole resonance peaks, each fairly insensitive to clipping. The existence of two quadrupole resonances for

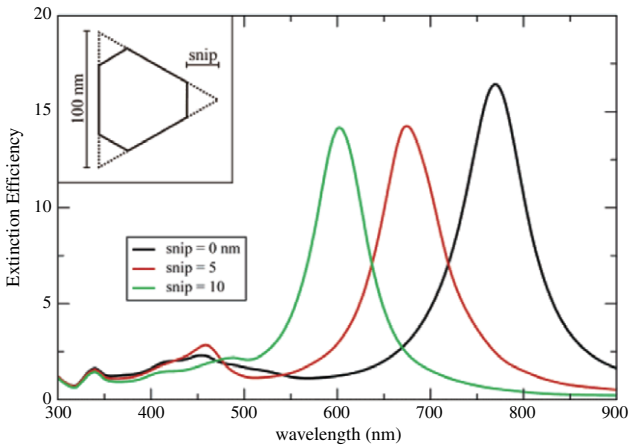

Figure 6. DDA calculation results of extinction efficiencies for trigonal prisms displaying varying degrees of clipping. (Results are an average over all incident polarizations.) For each prism, a strong dipole resonance, which for increasing values of snip distance is blue shifted, and two small quadrupole resonance peaks, each fairly insensitive to clipping, are seen. Reprinted figure with permission from [8]. Copyright 2003 by The American Chemical Society.

the silver triangular MNP is a surprise, given the fact that such resonances become insignificant for the silver spheroid MNPs described previously. Maximum field enhancements were seen for the dipole resonance at the tips of the perfect triangle, again asserting that sharper structures give rise to larger field enhancements.

Clusters and arrays of nanoparticles

It is natural to suspect that the interactions that result as MNPs are brought closer can further enhance local field intensities of relevance for SERS and nonlinear processes [26, 27] in general since such processes scale nonlinearly with the field intensity. It is also the case that some degree of waveguiding of SP excitations might occur in certain, engineered arrays [28, 29].

Full 3D FDTD simulations of multiple MNP configurations, while certainly possible, can require large computational domains and prohibitively large grids for accurate convergence. As a consequence there have been considerably more

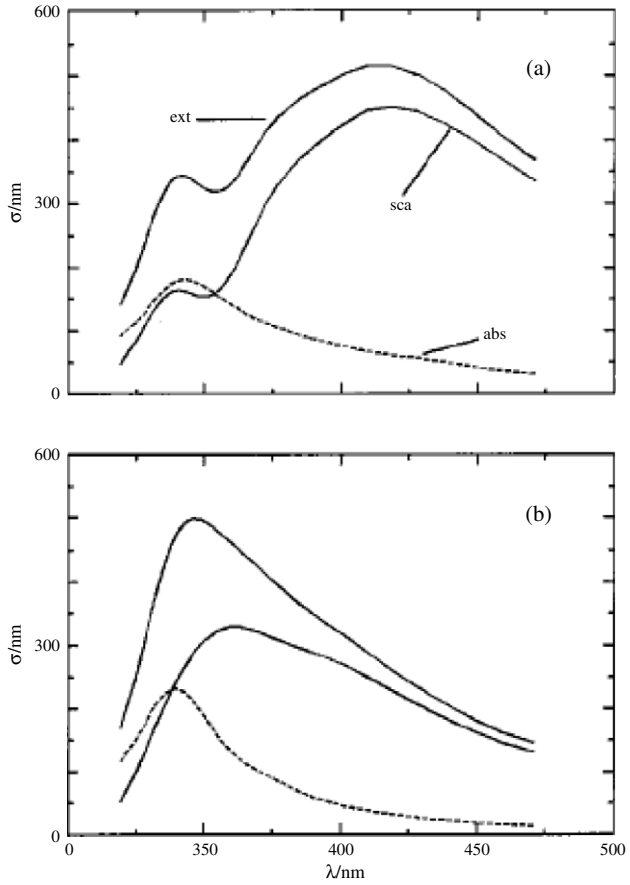

Figure 7. Absorption (abs.), scattering (sca.) and extinction (ext.) optical cross sections for a linear array of 4 silver cylinders, each with radius $a = 25$ nm. (a) 5 nm spacing between cylinders. (b) 25 nm spacing between cylinders. The smaller spacing cases give rise to a broadened, red-shifted dipolar resonance and a lower wavelength mixed dipolar/quadrupolar resonance. Reprinted figure with permission from [20]. Copyright 2003 by The American Physical Society.

studies of two-dimensional systems composed of infinitely extended metallic nanowires, e.g. [20, 27, 30, 31].

In [20], for example, Gray and Kupka use FDTD simulations to study isolated, paired, and funnel-shaped chain configurations of silver cylinders. It was shown that for light in the $\lambda = 300$–500 nm range, an isolated Ag cylinder behaves very much like a sphere with a similar radius, containing only a single, broad dipole resonance peak in the extinction cross section. The addition of cylinders in a closely packed linear array (5 nm spacing between 50 nm diameter cylinders) results in a red shift and broadening of the dipole peak and a mixed dipole/quadrupole resonance peak resulting from the coupling of SPs (see figure 7). Electric intensity enhancements were found to be larger than 100 between cylinders. It was possible to find some degree of propagation of energy down the chain, but the effect was relatively weak owing to absorption and scattering losses.

Finally, it is interesting to note a successful model capable of interpreting the optical spectra for MNPs and coupled systems of MNPs, known as the plasmon hybridization model of Nordlander and co-workers [32, 33]. The model is similar in spirit to quantum molecular orbital theory in that the plasmon response of a more complex structure can be considered as hybridizations of localized SPs on more elementary structures that interact due to the finite distance between them.

3.2. Surface plasmon polariton propagation in layered structures

So far we have discussed the properties of stationary LSP excitations on MNPs. It is also of interest to propagate or waveguide surface plasmon excitations within or on some structure. While arrays of MNPs may provide one avenue for such propagation [28, 29], the generation and manipulation of SPPs [5] in structures involving thin films is also of interest [34–37]. In such applications, it is desirable to have propagation distances as long as possible, though limiting factors can include energy loss due to scattering and absorption by the metal. In this section we consider several different proposed methods for increasing SPP propagation lengths, either by limiting absorption or minimizing the effect of scattering loss.

One common approach to increase propagation distances (relative to an isolated SPP on a semi-infinite metallic slab) is to couple the SPP into a waveguide composed of a thin (<100 nm) metallic core with symmetric or nearly symmetric dielectric cladding. The idea, suggested by Sarid in [38], is that for a thick metal, two degenerate transverse magnetic (TM) SPP modes exist, one at each metal/dielectric interface. However, as the thickness of the metal decreases, these TM modes can interfere to give rise to a long-range 'symmetric' mode (LR-SPP) and a short-range 'asymmetric' mode, where symmetry is with respect to the transverse magnetic field component within the metal. In the case of the LR-SPP, the field intensity is *decreased* within the metal, thereby reducing the effect of absorption, leading to predicted propagation lengths of more than an order of magnitude longer compared to isolated SPP values. LR-SPPs have been experimental verified [39, 40].

It is also possible to increase propagation distances using more asymmetric waveguide structures. Here we focus on one described in [41], where Lee and Gray use the FDTD approach to study the effects of varying metal and core thicknesses within an asymmetric SPP waveguide. The structure (see figure 8) involves a 3-layer *excitation* region composed of dielectric cladding layers 1 and 2, with $\varepsilon_2 > \varepsilon_1$, and a metallic core with complex, frequency-dependent ε_m and $\mathrm{Re}(\varepsilon_m) < 0$. Within this region, an SPP is launched along the layer 1/metal interface using a Kretschmann–Raether attenuated total reflection (ATR) [5] approach. Immediately adjacent to the excitation region is a 4-layer *propagation* region, in which an additional dielectric layer 3 is added beneath layer 2, where now $\varepsilon_2 > \varepsilon_1, \varepsilon_3$. For a fixed incidence angle ($\theta = 44.8°$) and wavelength ($\lambda = 532$ nm), the metal thickness, t_m, and layer 2 (core) thickness, d, are varied, and for each thickness the SPP propagation distance, L_x, is computed by fitting electric field intensities for a fixed distance above the metal surface to an exponential: $C\exp(-x/L_x)$. Sample FDTD results for the electric field intensities are given in figure 9 for a 30 nm

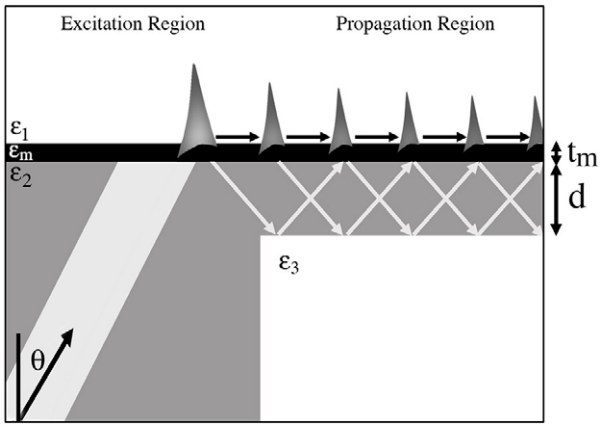

Figure 8. Waveguide structure of [41] and [42] including interpretation of SPP regeneration. Layers 1, 2, and 3 are dielectric materials with dielectric constants ε_1, ε_2, and ε_3. The thickness, d, of dielectric layer 2 underneath the metal is a key variable. Between layers 2 and 3 there is a thin metal film of thickness, t_m, and frequency-dependent, complex dielectric constant, ε_m. Reprinted figure with permission from [42]. Copyright 2008 by The American Physical Society.

silver film on glass ($\varepsilon_2 = 2.25$) with air for layers 1 and 3. Figure 9(a) corresponds to a standard SPP ($d = \propto$), and figure 9(b) corresponds to a 50 nm glass core thickness. It was found that small core (glass) and metal film thicknesses yielded the most dramatic enhancements, nearly 18× the standard SPP propagation length of ∼2 μm. The explanation presented in [41] is that SPPs excited at the layer 1/metal interface within the excitation region enter the adjacent propagation region, where the presence of the additional dielectric layer 3, with $\varepsilon_3 < \varepsilon_2$, gives rise to total internal reflection at the 2/3 interface. Reflected radiation, which would have otherwise been lost, is directed back towards the metal at the proper angle for regenerating SPPs.

In [42], a more extensive study of $L_x(d)$ was performed. For the same incident wavelength, $\lambda = 532$ nm, excitation angle, $\theta = 44.8°$, and a fixed metal thickness, $t_m = 30$ nm, an oscillatory behavior was seen in L_x as d increased from 0 to 650 nm (see figure 10), with maximum enhancements of nearly 30 times the standard SPP propagation distance. A frequency-domain modal analysis of the 4-layer propagation region based on Yeh's 2 × 2 matrix method [43] showed that the dependence of L_x on d is due to the tuning of d to different allowed TM waveguide modes.

Another asymmetric SPP waveguide involves adding a polymer ridge with finite width, w, and thickness, h, atop a metal layer supported by glass, for example [44–46]. Theoretical studies using finite element techniques [46] showed enhanced SPP propagation lengths and field confinement at telecom wavelengths for optimal values of ridge dimensions w and h on a gold surface. It is also possible to efficiently guide light in complementary waveguides, composed of dielectric cores with subwavelength widths in gold and silver claddings [47, 48].

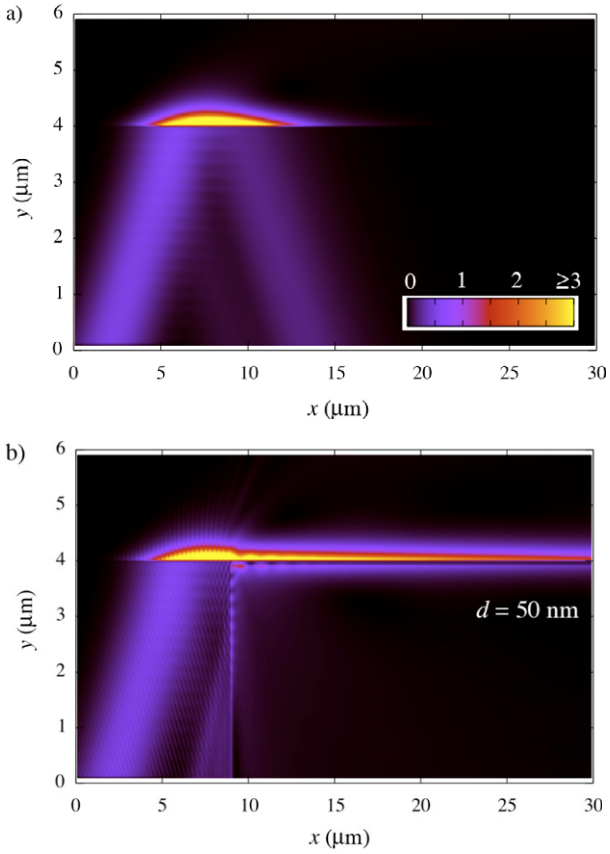

Figure 9. FDTD results for the time-averaged electric field intensities for the structure in figure 8 with (a) $d = \infty$ (conventional ATR) and (b) $d = 50$ nm. In each case, the incident field intensity is given by $\langle E^2_{inc}\rangle_t = 0.5$ V^2 m^{-2}, and the maximum field intensity occurs in the excitation region near $x = 7$ μm, for which $\langle E^2\rangle_t = 10$ V^2 m^{-2}. However, intensities $\geqslant 3$ V^2 m^{-2} are represented by yellow online, white in print, as indicated in (a).

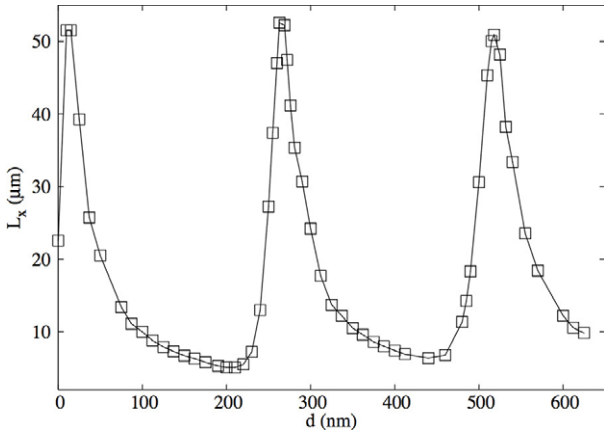

Figure 10. R-SPP propagation length L_x, as a function of the glass core thickness, d, for the waveguide structure in figure 8 [41, 42]. L_x determined by fitting electric field intensities at a fixed distance above the metal surface to $C\exp(-x/L_x)$. Adapted from [42].

3.3. Periodic hole arrays in metal films

In 1998 Ebbesen *et al* [49] presented experimental results showing that periodic arrays of subwavelength holes in a metal

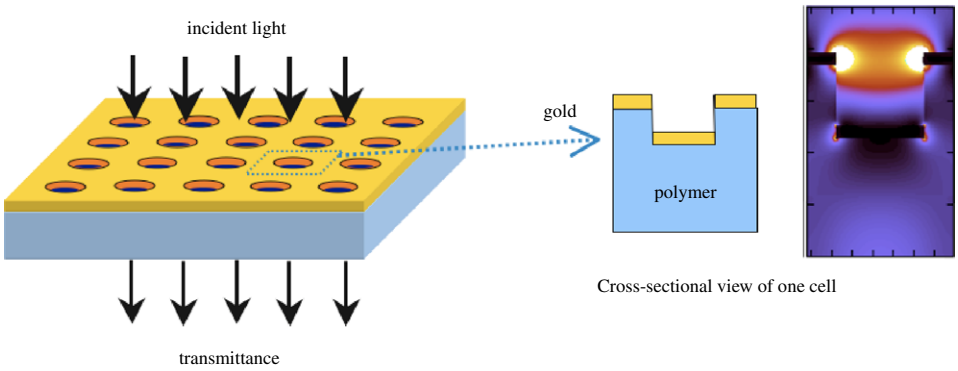

Figure 11. Nanohole or nanowell arrays exhibit complex light transmission spectra of relevance to chemical and biological sensing. High and localized electromagnetic field intensities result from surface plasmon excitations (right-most image). The specific system illustrated is a depiction of the plasmonic crystal developed by Rogers, Nuzzo and their co-workers [58].

film can exhibit structured light transmission spectra with peak maxima corresponding to a surprising amount of transmission in comparison with expectations based on Bethe–Bouwkamp theory [50, 51]. See figure 11 for a schematic illustration of the type of system under consideration. Bethe–Bouwkamp theory is an analytical treatment of light transmission by a hole in a perfect metal that cannot support SP excitations. This extraordinary optical transmission (EOT) phenomenon is also very sensitive to the nature of any substrate placed over the holes and so many researchers have explored the possibility of developing chemical and biological sensors based on such systems [52].

Ebbesen *et al* concluded the EOT observed for hole arrays in real metals was related, in part, to the periodic analog of SPPs, which we will term SPP Bloch waves. These waves may be understood as standing waves formed from superpositions of counter-propagating SPPs excited via a grating coupling mechanism. For a square array of holes with periodicity P in a metal film with dielectric constant $\varepsilon_{\mathrm{m}}(\lambda)$, simple arguments lead to the prediction that SPP Bloch waves would occur near the discrete incident wavelengths, $\lambda = \lambda_{\mathrm{SPP-BW}}$ [49, 53] such that

$$\lambda_{\mathrm{SPP-BW}} = \frac{P}{\left(j^2 + k^2\right)^{1/2}} \left(\frac{\varepsilon_X \varepsilon_{\mathrm{m}}(\lambda_{\mathrm{SPP-BW}})}{\varepsilon_X + \varepsilon_{\mathrm{m}}(\lambda_{\mathrm{SPP-BW}})} \right)^{1/2}, \quad (14)$$

with j and k being integers. In equation (14), ε_X denotes the dielectric constant of the material interfacing with the metal, and there can be SPP Bloch waves associated with either the top or bottom interface.

While these systems appear to be very simple, a variety of other phenomena can occur including more diffractive features such as Rayleigh anomalies (also sometimes called Wood anomalies) which can be close to the wavelengths predicted by equation (14), as well as LSP excitations about the holes and waveguide modes. The condition for a Rayleigh anomaly is simply

$$\lambda_{\mathrm{RA}} = \frac{P}{\left(j^2 + k^2\right)^{1/2}} (\varepsilon_X)^{1/2}. \quad (15)$$

As a consequence of all the possible phenomena that can occur in these systems, there has been some debate in the literature about the relative importance of the various features contributing to EOT. Some researchers also suggested a new type of surface wave that is unrelated to SPPs, which they called a composite diffracted evanescent wave (CDEW), as being important in EOT [54, 55]. However, subsequent physical and mathematical analysis, coupled with FDTD simulations, have shed some doubt on the existence of such waves [56].

It is relatively straightforward to apply periodic boundary conditions to the three-dimensional FDTD equations of section 2.2 and to study such hole arrays systems with the incident light coming up normal to the surface. (While possible, it is technically more challenging to study non-normal incidence on periodic structures with the FDTD method, especially if a range of wavelengths is of interest [10].) Here we will discuss three particular FDTD studies of light transmission by periodically structured metallic nanosystems in three dimensions [57–59]. Other three-dimensional FDTD studies of such systems include [60–63].

In the first study, Chang *et al* [57] examined square arrays of 200 nm diameter holes in 100 nm thick gold films on top of a glass substrate (with air above the hole system), with incident light ranging from $\lambda = 500$–1000 nm. A normalized transmission is defined as $T_n = (F_{\mathrm{tot}} - F_{\mathrm{film}})/(I_{\mathrm{inc}} \pi a^2)$, where F_{tot} is the transmitted flux for the hole system integrated over the top area of the unit cell, F_{film} is the same quantity but for the problem of a gold film with no holes in it, I_{inc} is the incident flux and a is the radius of a hole. This transmission is displayed for the specific hole array system of [57] in figure 12. It turns out that many of the transmission minima in figure 12 correlate well with the zero order SPP Bloch wave positions predicted by equation (14). Intuitively, one can imagine energy being channeled into these SPPs which, to zero order, do not directly transmit light because of their evanescent character. The reality is, however, that these SPPs are coupled to light that is being directly transmitted both through the holes and through the film. The nature of this coupling turns out to be well described by Fano's model of a discrete state interacting with a continuum state which leads to asymmetric transmission profiles that include a minimum followed by a maximum [64]. This idea was first suggested in [65] and [66]. In the present,

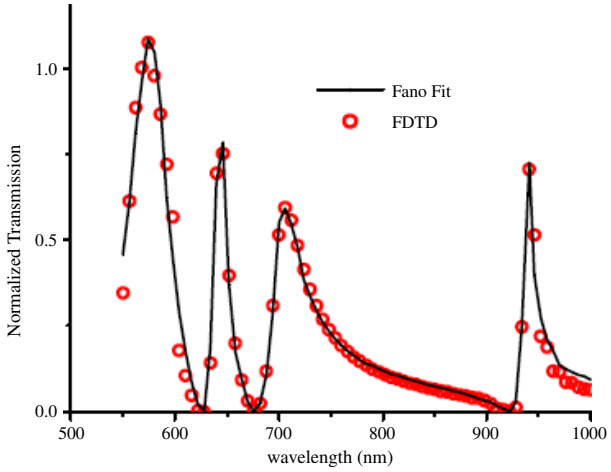

Figure 12. Normalized optical transmission for the periodic hole array in a gold film discussed in the text. Reprinted figure with permission from [57]. Copyright 2005 by the Optical Society of America.

classical electrodynamics context [57] showed that a multiple Fano resonance model involving just a few parameters could accurately fit the FDTD results, as also indicated in figure 12. Reference [57] also showed, in addition to SPP-BWs and RAs, that LSP excitations around the holes can play an important role. LSP excitations around holes are complementary to the LSP excitations in nanoparticles and can exhibit similar properties [35, 67, 68].

The second periodic hole array study of interest is the combined experimental and theoretical study of Stewart *et al* [58], which involved depositing a thin gold film over a polymer structure that was imprinted with cylindrical wells. The result was a gold film on top of the polymer with a square hole array, and at the bottom of each hole was a gold disk, as schematically illustrated in figure 11. As in [57], a variety of transmission features were identified. However, whereas reference [57] had just air on top of the array, reference [58] examined how the transmission features change as the refractive index (RI) of the material on top varies. It was found that some spectral features were far more sensitive than others, and the origins of this sensitivity were traced to plasmon resonances connecting top hole structures with the bottom disk structures. One such resonance is illustrated in the right-hand side panel of figure 11. Another feature of this work was that to obtain good agreement with experiment, it was necessary to introduce small imperfections into the theoretical structure. Specifically, when some excess pile up of gold around the edges of the disk was included, which was consistent with TEM images of the actual sample, the transmission of the most sensitive spectral structure changed by more than 10% becoming in better accord with experiment.

The final hole array study we wish to highlight was another combined experimental and theoretical effort. In this work, McMahon *et al* [59] examined simple square hole arrays in gold films on glass, much like those in the first study we noted of Chang *et al* [57]. As in the work of Stewart *et al* [58], though, the sensitivity of the transmission to the RI of a substrate was examined. It was shown, in particular, that it is possible to engineer features of the array, e.g. its periodicity, such that particularly sensitive spectral peaks occur in a specific RI range of interest. This suggests the possibility of tailoring the design hole array systems for sensing in particular RI ranges. The basis for this was the concept of coupling an SPP Bloch wave with a Rayleigh anomaly. Equations (14) and (15) could be used to predict an optimal periodicity such that an SPP Bloch wave and Rayleigh anomaly occurred at the same incident wavelength for a given upper substrate RI. With such an array, when one considers a range of samples with RI passing through this particular RI one will see a strong rise in the transmission. This idea was validated and explored further with FDTD calculations and also demonstrated experimentally [59].

4. Concluding remarks

We discussed the theory and modeling of light interactions with metallic nanostructures, placing some emphasis on results obtained with a rigorous computational electrodynamics method, the FDTD method [9, 10].

Metallic nanostructures and hybrid structures containing them are of key importance to the exciting area of nanoscience called nanophotonics [1–4]. Of particular interest is the creation and manipulation of surface plasmon (SP) excitations, which at the continuum electrodynamics level are certain evanescent surface wave solutions to Maxwell's equations. SPs are localized in one direction and can be quite intense. Such properties make them of interest for a variety of practical applications including, for example, chemical and biological sensing [52].

Analytical models ranging from exact solutions to Maxwell's equations for spheroids and solutions appropriate to certain limits, e.g. the quasistatic limit, have provided the basic foundations for our understanding of SPs. However, the greater variety of particle shapes and complex metallic structures that can now be fabricated using nanotechnology cannot be quantitatively described with such approaches. When correctly applied and complemented by careful physical analysis, the FDTD method can provide insight into these systems. In this review we discussed the results of a variety of (mostly) FDTD studies ranging from relatively simple metal nanoparticles as in [24] dominated by local surface plasmon excitations to relatively complex periodically nanostructured systems such as in [57–60] where a variety of plasmonic and diffractive phenomena compete.

Acknowledgments

The work at Argonne National Laboratory was supported by the US Department of Energy, Basic Energy Sciences, under contract No. DE-AC02-06CH11357.

References

[1] Prassad P N 2004 *Nanophotonics* (New York: Wiley)
[2] Kawata S, Ohtus M and Irie M 2002 *Nano-Optics* (New York: Springer)

[3] Barnes W L, Dereux A and Ebbesen T W 2003 *Nature* **424** 824
[4] Maier S A and Atwater H A 2005 *J. Appl. Phys.* **98** 011101
[5] Raether H 1988 *Surface Plasmons on Smooth and Rough Surfaces and on Gratings* (New York: Springer)
[6] Bohren C F and Huffman D R 1983 *Absorption and Scattering of Light by Small Particles* (New York: Wiley)
[7] Mie G 1908 *Ann. Phys.* **25** 377
[8] Kelly K L, Coronado E, Zhao L L and Schatz G C 2003 *J. Phys. Chem.* B **107** 668
[9] Yee K S 1966 *IEEE Trans. Antennas Propag.* **14** 302
[10] Taflove A and Hagness S C 2005 *Computational Electrodynamics: The Finite Difference Time-Domain Method* 3rd edn (Norwood, MA: Artech House)
[11] Draine B T and Flateau P J 1994 *J. Opt. Soc. Am.* A **11** 1491
[12] Yang W-H, Schatz G C and Van Duyne R P 1995 *J. Chem. Phys.* **103** 869
[13] Moreno E, Erni D E, Hafner C and Vahldieck R 2002 *J. Opt. Soc. Am.* A **19** 101
[14] Kottmann J P, Martin O J F, Smith D R and Schultz S 2000 *Opt. Express* **6** 213
[15] Ewe W-B, Chu H-S and Li E-P 2007 *Opt. Express* **15** 18200
[16] Themistos C, Azizur Rahman B M, Rajarajan M, Rakocevic V and Grattan K T V 2006 *J. Lightwave Technol.* **24** 5111
[17] Johnston B P and Christy R W 1972 *Phys. Rev.* B **6** 4370
[18] Lynch D and Hunter W R 1985 *Handbook of Optical Constants* ed E D Palik (New York: Academic)
[19] Ziolkowski R W and Tanaka M 1999 *J. Opt. Soc. Am.* A **16** 930
[20] Gray S K and Kupka T 2003 *Phys. Rev.* B **68** 045415
[21] Berenger J P 1996 *IEEE Trans. Antennas Propag.* **51** 110
[22] Gedney S D 1996 *IEEE Trans. Antennas Propag.* **44** 1630
[23] Merewether D E, Fisher R and Smith F W 1980 *IEEE Trans. Nucl. Sci.* **27** 1829
[24] Liu M, Guyot-Sionnest P, Lee T-W and Gray S K 2007 *Phys. Rev.* B **76** 235428
[25] Jin R, Cao Y, Mirkin C A, Kelly K L, Schatz G C and Zheng J C 2001 *Science* **294** 1901
[26] Panoiu N C and Osgood R M Jr 2004 *Nano Lett.* **4** 2427
[27] Wang X, Schatz G C and Gray S K 2006 *Phys. Rev.* B **74** 195439
[28] Maier S A, Kik P G, Atwater H A, Meltzer S, Harel E, Koel B E and Requicha A A G 2003 *Nat. Mater.* **2** 229
[29] Zou S and Schatz G C 2006 *Phys. Rev.* B **74** 125111
[30] Kottmann J P and Martin O J F 2000 *Opt. Express* **8** 655
[31] Sukharev M and Seideman T 2007 *J. Chem. Phys.* **126** 204702
[32] Prodan E and Nordlander P 2003 *J. Chem. Phys.* **120** 5444
[33] Prodan E, Radloff C, Halas N J and Nordlander P 2003 *Science* **302** 419
[34] Dostalek J, Kasry A and Knoll W 2007 *Plasmonics* **2** 97
[35] Yin L, Vlasko-Vlasov V K, Rydh A, Pearson J, Welp U, Chang S-H, Gray S K, Schatz G C, Brown D E and Kimball C W 2004 *Appl. Phys. Lett.* **85** 467
[36] Hochberg M, Baehr-Jones T, Walker C and Scherer A 2004 *Opt. Express* **12** 5481
[37] Bozhevolnyi S, Volkov V S, Devaux E, Laluet J-Y and Ebbesen T W 2006 *Nature* **440** 508
[38] Sarid D 1981 *Phys. Rev. Lett.* **47** 1927
[39] Craig A E, Olson G A and Sarid D 1983 *Opt. Lett.* **8** 380
[40] Berini P, Charbonneau R, Lahoud N and Mattiussi G 2005 *J. Appl. Phys.* **98** 043109
[41] Lee T-W and Gray S K 2005 *Appl. Phys. Lett.* **86** 141105
[42] Montgomery J M and Gray S K 2008 *Phys. Rev.* B **77** 125407
[43] Yeh P 1988 *Optical Waves in Layered Media* (New York: Wiley)
[44] Steinberger B, Hohenau A, Ditlbacher H, Stepanov A L, Drezet A, Aussenegg F R, Leitner A and Krenn J R 2006 *Appl. Phys. Lett.* **88** 094104
[45] Reinhard C, Passinger S and Chichkov B N 2006 *Opt. Lett.* **9** 1307
[46] Holmgaard T and Bozhevolnyi S I 2007 *Phys. Rev.* B **75** 245405
[47] Veronis G and Fan S 2005 *Appl. Phys. Lett.* **87** 131102
[48] Lee T-W and Gray S K 2005 *Opt. Express* **13** 9652
[49] Ebbesen T W, Lezec H J, Ghaemi H F, Thio T and Wolff P A 1998 *Nature* **391** 667
[50] Bethe H A 1944 *Phys. Rev.* **66** 163
[51] Bouwkamp C J 1950 *Philips Res. Rep.* **5** 321
[52] Stewart M E, Anderton C R, Thompson L B, Maria J, Gray S K, Rogers R A and Nuzzo R G 2008 *Chem. Rev.* **108** 494
[53] Ghaemi H F, Thio T, Grupp D E, Ebbesen T W and Lezec H J 1998 *Phys. Rev.* B **58** 6779
[54] Lezec H and Thio T 2004 *Opt. Express* **12** 3629
[55] Gay G, Alloschery O, Viaris de Lesegno B, O'Dwyer C, Weiner J and Lezec H J 2006 *Nat. Phys.* **2** 262
[56] Garcia-Vidal F J, Rodrigo G and Martin-Moreno L 2006 *Nat. Phys.* **2** 790
[57] Chang S-H, Gray S K and Schatz G C 2005 *Opt. Express* **13** 3150
[58] Stewart M E, Mack N H, Malyarchuk V, Soares J A N T, Lee T-W, Gray S K, Nuzzo R G and Rogers J A 2006 *Proc. Natl Acad. Sci. USA* **103** 17143
[59] McMahon J M, Henzie J, Odom T W, Schatz G C and Gray S K 2007 *Opt. Express* **15** 18119
[60] Hohng S G, Yoon Y C, Kim D S, Malyarchuk V, Muller R, Lienau Ch, Park J W, Yoo K H, Kim J, Ryu H Y and Park Q H 2002 *Appl. Phys. Lett.* **81** 3239
[61] Muller R, Malyarchuk V and Lienau Ch 2003 *Phys. Rev.* B **68** 205415
[62] Egorov D, Dennis B S, Blumberg G and Haftel M I 2004 *Phys. Rev.* B **70** 033404
[63] Ruan Z and Qiu M 2006 *Phys. Rev. Lett.* **96** 233901
[64] Fano U 1961 *Phys. Rev.* **124** 1866
[65] Sarrazin M, Vigneron J-P and Vigoureux J-M 2003 *Phys. Rev.* B **67** 085415
[66] Genet C, van Exter M P and Woerdman J P 2003 *Opt. Commun.* **225** 331
[67] Wannemacher R 2001 *Opt. Commun.* **195** 107
[68] Prikulis J, Hanarp P, Olofsson L, Sutherland D and Kall M 2004 *Nano Lett.* **4** 1003